European Journal of Orthodontics 33 (2011) 608–612
doi:10.1093/ejo/cjq112
Advance Access Publication 3 December 2010

A comparison of finite element analysis with *in vitro* bond strength tests of the bracket–cement–enamel system

T.J. Algera*, A.J. Feilzer**, B. Prahl-Andersen* and C.J. Kleverlaan**
Departments of *Orthodontics and **Dental Materials Science, Academic Centre for Dentistry Amsterdam, The Netherlands

Correspondence to: T.J. Algera, Academic Centre for Dentistry Amsterdam, Department of Orthodontics, Louwesweg 1, 1066 EA Amsterdam, The Netherlands. E-mail: talgera@acta.nl

SUMMARY The aim of this study was to determine the *in vitro* shear bond strength (SBS) and tensile bond strength (TBS) of 45 metal brackets bonded with Transbond XT to bovine enamel. The SBS was determined by loading the short and the long sides of the bracket base. Testing took place after storage of the specimens for 72 hours in water at 37°C. Fractures were analysed with the adhesive remnant index (ARI) and scanning electron microscope (SEM). The stresses in the system were analysed with finite element (FE) analysis models of the experimental set-up to identify the initial fracture point and the stress distribution at fracture. Statistical analysis of bond strengths was performed using analysis of variance (ANOVA) and the Tukey's *post hoc* test ($P < 0.05$). The ARI scores were analysed using Kruskal–Wallis one-way ANOVA on ranks.

ANOVA showed significant differences between the three experiments. Loading the short side of the bracket resulted in the highest average bond strength. Tensile loading gave the lowest results. FE models supported the bond strength findings and SEM. FE analysis revealed peak stresses in the cement during loading, confirming that shear testing is sensitive to loading angles. The stress distribution over the bracket–cement–enamel system is not homogeneous during loading. Fractures are initiated at peak stress locations. As a consequence, the size of the bonding area is not predictive of bond strength. The bracket design and the mode of loading may be of greater relevance.

Introduction

Bracket bond failure during orthodontic treatment is a recurring event with the consequence that the bracket must be rebonded. This influences treatment time. Bracket failures are mostly explained by interference with contact loading, incorrect performance of the bonding procedure, fatigue of the bonding material, or a combination of these factors (O'Brien *et al.*, 1989). To obtain an insight into the strength of the bracket–cement–enamel bond, *in vitro* tests are performed. With these tests, the force necessary to debond a bracket is measured. The values are measured as force [Newton (N)] but most often reported as strength [Megapascals (MPa)], which is calculated by dividing the force by the bonding area. Furthermore, the enamel specimen is usually examined under a microscope to identify the mode of failure, cohesive, or adhesive. This mode of failure, which is represented in the adhesive remnant index (ARI), should provide information on the weakest part of the bonding system (Årtun and Bergland, 1984).

The variance among reported bond strength values in different studies is probably caused by the number of variables that are involved in these tests. This makes interpretation and comparison with existing data difficult. As mentioned, bond strength is reported in MPa, which assumes that the complete bonding area is equally loaded at fracture. According to finite element (FE) analysis, this is unlikely. Katona (1997) showed that the force distribution during shear, tensile, or rotational testing is not homogeneous. It is more likely that a fracture, during loading, starts at a weak point in the system, usually a void or crack, or at the border of the bracket (Higg *et al.*, 2001). Because of the brittle nature of the cement (Higg *et al.*, 2001), these initial cracks lead to complete fracture and debonding of the bracket. The elastic property of the bracket and the cement used play a role in the debonding as these will affect the distribution of the load into the bracket and adhesive. This is confirmed by the difference in bond strength between ceramic and stainless steel brackets bonded with the same cement (Haydar *et al.*, 1999). It would therefore be beneficial to obtain an insight into the stress distribution prior to debonding and the location of fracture initiation. Together with a knowledge of the fracture propagation pattern and the force measured at debonding, this can lead to a better understanding of bracket bond failures and eventually to prevention of this problem.

The aim of this study was to determine the fracture mechanisms of bracket debonding using FE analysis on *in vitro* bond strength test specimens and scanning electron microscope (SEM) photomicrographs.

Materials and methods

The tensile bond strength (TBS) and shear bond strength (SBS) of a bracket–cement–enamel system were measured

and their fractures were analysed using SEM. The obtained TBS and SBS were used as input for FE modelling and analysis of the test specimens.

Specimen preparation

Enamel specimens were prepared from bovine teeth, obtained from 2-year-old cattle. The crowns of the teeth were sectioned from the roots and embedded in polymethyl methacrylate.

Before bonding, the buccal surfaces were ground with sandpaper until grit 1200, ensuring a standard smooth bonding surface. Mesh-based central upper incisor brackets (Mini Twin; A Company Orthodontics, San Diego, California, USA; size 3.0 × 4.2 mm) were bonded using Transbond XT (3M Unitek, Monrovia, California, USA). Pre-treatment of the bonding area was carried out according to the manufacturers' instructions and consisted of 35 per cent phosphoric acid etching (Ultradent Products, South Jordan, Utah, USA) followed by the application of a thin layer of adhesive resin (3M Unitek). Light curing was performed using an Elipar Trilight curing unit (3M-Espe Dental Products, Seefeld, Germany) in a standard mode at 750 mW/cm^2. The specimens were stored in tap water at 37°C for 72 hours. The specimens were prepared and tested by one experienced researcher (TJA).

TBS and SBS determination

TBS was determined as described by Algera *et al.* (2005). The specimens were attached to the crosshead of a universal testing machine (Hounsfield Ltd, Redhill, Surrey, UK) using a 0.020 inch stainless steel wire bent in a U-form and tied with a harness ligature to the bracket. The free ends of the wire were clamped in the connecting piece of the crosshead. A hinge in the connecting piece together with the round wire, allowed vertical alignment of the specimen, which is required for homogeneous stress distribution during testing. SBS was determined in two directions. The brackets were loaded at the short and long sides. For both tests, the specimens were placed in a brass block in which the bracket was located exactly at the edge of the holder as described by Algera *et al.* (2008a). Forty-five specimens were tested resulting in three groups of 15 specimens each. The bond strength tests were carried out in a universal testing machine at a crosshead speed of 0.5 mm/minute. Average TBS and SBS were calculated by dividing the measured load at fracture by the bonding area.

After testing, fracture mode was scored using the ARI (Årtun and Bergland, 1984) to identify the weakest point in the bracket–cement–enamel system. A score of 0 indicates that no adhesive is left on the enamel, 1 less than half of the adhesive remained, 2 more than half of it remained, and 3 all adhesive remained on the enamel surface. The scores were determined with a stereomicroscope at a magnification of ×25.

Statistical analysis

One-way analysis of variance (ANOVA) was used to test the effect of the different test methods and Tukey's *post hoc* test to determine individual differences. Differences in ARI scores were analysed using the Kruskal–Wallis one-way ANOVA on ranks. A level of $P < 0.05$ was considered significant. The software used was SigmaStat Version 3.0 (SPSS Inc., Chicago, Illinois, USA).

SEM analysis of the specimens

After fracture, one specimen of each test mode was selected for SEM analysis of the fracture surface. These specimens were gold plated using a sputter coater (Edwards Sputter Coater S 150B; Edwards and Philips, Crawley, Sussex, UK). Examination was carried out with a SEM (20 XL; Philips, Eindhoven, The Netherlands) at ×25 magnification.

FE analysis

A three-dimensional simplified FE model with the three loading modes of the bracket–cement–enamel system was created. The FE modelling was carried out with FEMAP software (version 8.10; ESP, Maryland Height, Missouri, USA) and the analysis with CAEFEM 7.3 (CAC, West Hills, California, USA). The dimensions of the enamel block representing an abutment tooth were length 6.0 mm, width 5.0 mm, and height 1.0 mm. The cement layer was 4.2 mm long, 3.0 mm wide, and 200 μm high. The dimensions of the bracket–cement–enamel system are shown in Figure 1. The models were composed of 23 392 parabolic hexagonal solid elements. The material properties (Table 1) were assumed to be isotropic, homogenous and linear elastic (Geng *et al.*, 2001; Walker *et al.*, 2003). The nodes at the bottom of the enamel were fixed (no translation or rotation in any direction). To make the results comparable, a standardized load of 100 N was applied at various points (Figure 2). With the peak stress results of the virtually loaded models and the average bond strength results of the *in vitro* tests, the peak stresses inside the specimens at fracture could be calculated.

Results

The results of the three bond strength tests are summarized in Table 2. The lowest bond strength values were observed with the tensile test, while the shear tests resulted in significantly higher bond strength values. Comparison of the shear tests showed that loading the short side gave higher fracture bond strength values compared with loading the long side. The ARI scores (Table 3) of the three test modes did not significantly differ. The average score was between 2 and 2.5 indicating that most of the adhesive remained on the enamel. After fracture, the specimens were also studied with SEM. The specimens loaded on the long or short side

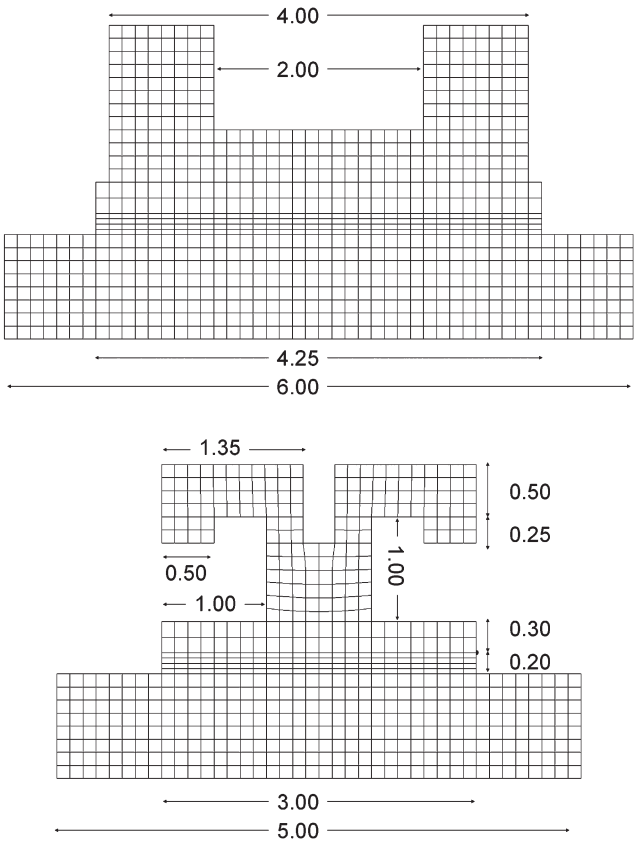

Figure 1 Geometric measurement of the bracket–cement–enamel system. The upper drawing shows the occlusal view. The lower drawing is from the mesial or distal side.

Table 1 The elastic moduli and Poissons ratio of the materials used in the finite element model.

Material	Young's modulus (MPa)	Poisson's ratio
Stainless steel	210 000	0.3
Enamel	84 000	0.3
Composite (Transbond XT)	5000	0.3

showed a fracture pattern, which started adhesively between the cement and the bracket and then changed into a cohesive fracture (Figure 3A and 3B). The tensile loaded specimens showed a completely adhesive fracture between the bracket and the cement (Figure 3C).

The FE model represents a stainless steel bracket bonded to enamel with a composite cement. The models with the different loading modes, (A) tensile, (B) long side, and (C) short side, are shown in Figure 2. The sectional views of the cement layer depending on the three loading modes are shown in Figure 4. The results obtained show that the force distribution of the three different loading modes was not homogeneous. Tensile loading resulted in the highest peak stress located at the short sides of the bracket (25.8 MPa), while loading the system on the long and short sides resulted

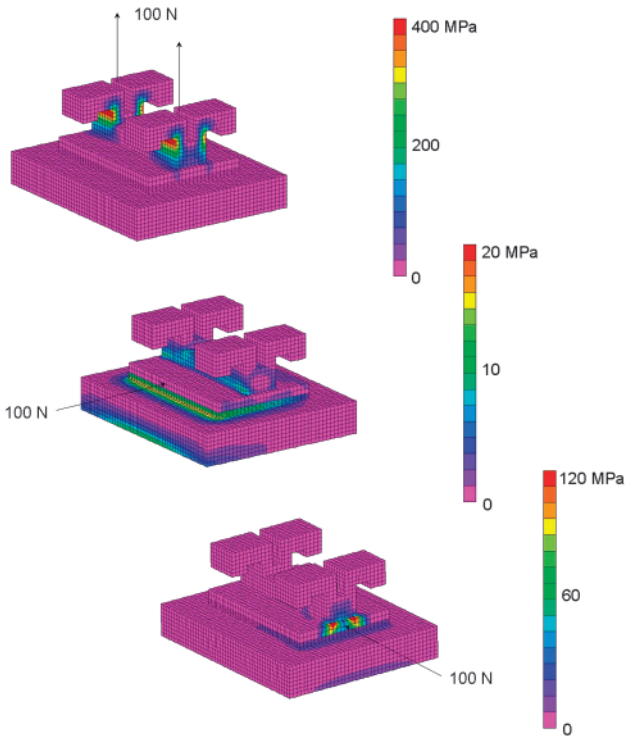

Figure 2 Finite element models of the bracket–cement–enamel system. The loading vector is indicated with an arrow. All models are loaded with 100 N. The resulting stress distributions during loading are shown in Megapascals (MPa).

Table 2 The average loading forces and bond strengths reported in Newton (N) and Megapascal (MPa), respectively, together with the standard deviations.

	Force (N)	Strength (MPa)	Calculated debonding peak stress (MPa)
Tensile strength	69.4[a] (5.7)	5.7[a] (1.8)	17.9
Shear strength long side	117.4[b] (9.6)	9.6[b] (2.5)	18.7
Shear strength short side	153.9[c] (12.4)	12.4[c] (2.8)	31.1

Lower case letters indicate a significant difference between the tests at a level of 0.05. In the third column, the peak stresses are calculated on basis of the finite element models loaded with 100 N. The results of the shear tests are calculated with a loading angle of 0 degrees.

Table 3 Adhesive remnant index scores.

Test	0	1	2	3	Average
Shear long	1	3	4	7	2.3
Shear short	0	2	7	6	2.3
Tensile	0	2	6	7	2.1

in 15.9 and 20.6 MPa, respectively. With these results, the peak forces responsible for the fracture of the *in vitro* specimens could be calculated (Table 2). Based on the experimental data, it was expected that loading on the short

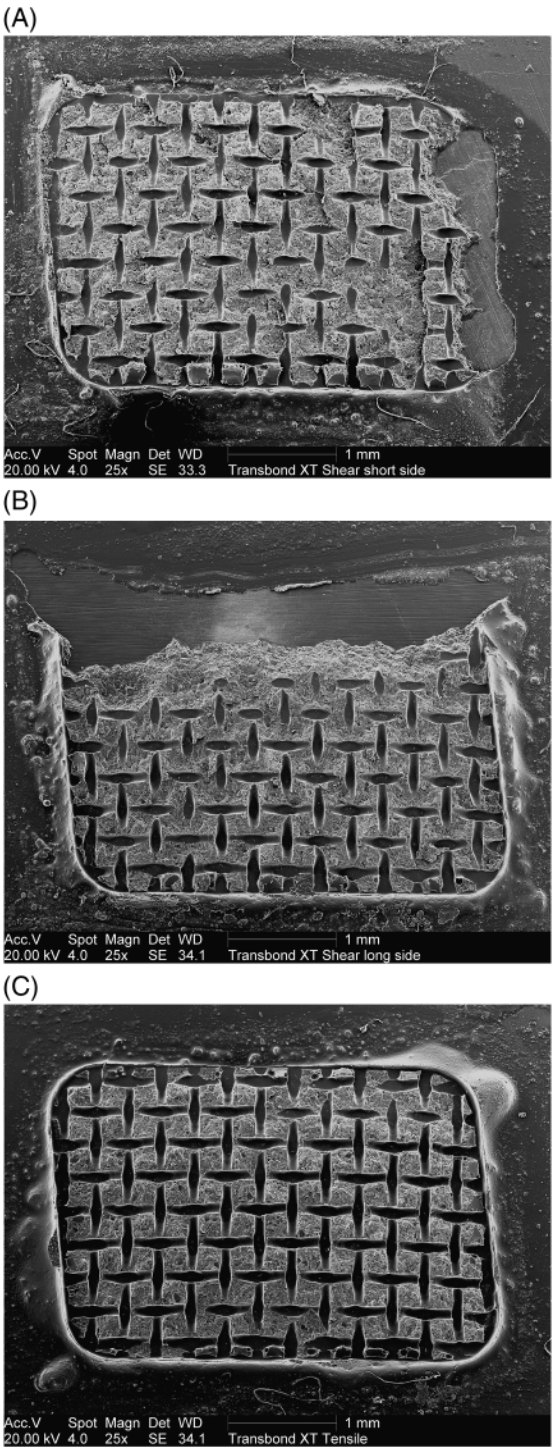

Figure 3 Photomicrographs showing the bonding areas of the debonded specimens. Specimen A underwent a shear load at the short left side, specimen B was shear loaded at the long underside, and specimen C was loaded in a tensile direction. The fracture patterns resulting from both shear tests give a similar view. The fracture starts cohesively at the pressure side and produces an adhesive failure at the far end of the bonding area. Difference between the two is the presence of fracture lines in the specimen loaded at the short side, which run perpendicular to the loading direction. These lines are not present in the specimen loaded at the long side. The specimen loaded in a tensile manner does not show a clear fracture pattern. The start of crack initation at one of the short sides is most likely.

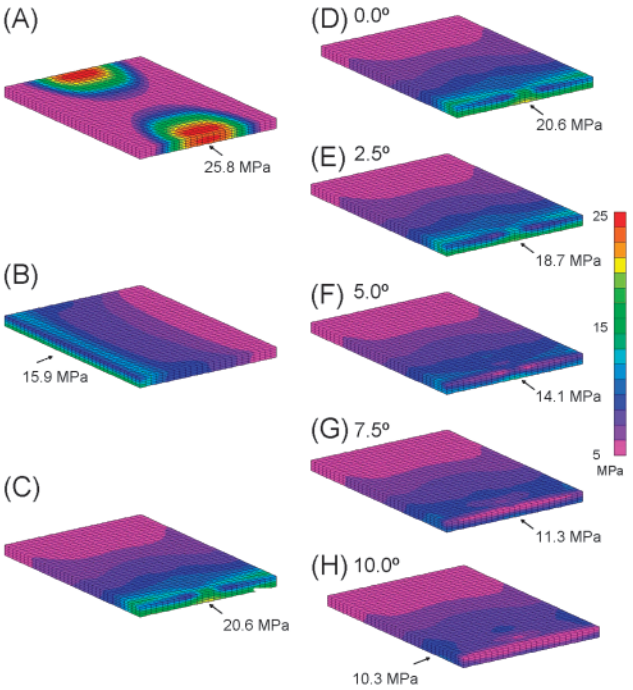

Figure 4 Stress distributions in the cement layer during loading. The colours represent the actual stress when the bracket is loaded with 100 N. Figures A, B, and C show the cements of the three different loading procedures and D, E, F, G, and H shear loading at the short bracket side under different angulation.

side would result in the lowest peak stress. Because this was not found in the FE model, the load angle was varied between 0 and 10 degrees. The calculations for the different loading angles resulted in different stress distributions and peak stresses. The results are graphically depicted in Figure 4D–4H.

Discussion

In vitro bond strength is tested both in tensile and in shear. The latter test was performed in two modes, at the short and long side of the bracket base. Significant differences in bond strength between tensile and shear tests are reported (Katona and Long, 2006). The significant differences, measured between the two shear tests, that can occur is in general not well recognized. The location of loading is usually not reported in the literature. The results clearly demonstrate that the location of the load and consequent stress distribution inside the bracket–cement–enamel system is an important parameter in strength testing.

In the study by Algera *et al.* (2008b), specimens consisting of small stainless steel buttons with a round base bonded with Transbond XT to bovine enamel were investigated. The SBS for the bracket–cement–enamel system was found to be 23.7 MPa. This was higher compared with the values of the present study (9.6 and 12.4 MPa for loading the long and short sides, respectively). Apparently, small stainless steel buttons with a round base distribute the applied load

better resulting in relatively lower local peak stress and as a result higher SBS. That stress distribution plays an important role in tensile and shear testings has already been recognized (Katona, 1997). For that reason, tensile and shear testings are commonly performed on small specimens (less than 1 mm^2), e.g. micro TBS and SBS testings.

In order to understand the peak stress and distribution during loading of the bracket–cement–enamel system, a FE model was created. When a standardized tensile load of 100 N was applied to the model, a peak stress of 25.8 MPa within the cement layer was found. Experimentally, an average load fracture of 69.4 N was observed. From these values, it can be calculated that the experimental peak stress within the cement layer causing failure was (69.4/100.0) × 25.8 = 17.9 MPa. For SBS with loading on the long side, an experimental peak stress of 18.7 MPa was calculated. These two values are in good agreement and close to the 23.7 MPa previously observed by Algera *et al.* (2008b). The SBS with loading on the short side resulted in an experimental peak stress of 31.1 MPa, which was much higher compared with the two other values. An explanation based on stiffness, curvature of the bracket, or cement layer thickness could not completely clarify this observation. The design of the bracket revealed that the base and wings had the same dimensions (Figure 1). Therefore, if the edge of bracket base and wing tip are in contact with the base plate of the shear bond testing device, the bracket base is always exactly parallel to the loading direction. The shear bond test when the bracket was loaded on the short side is in this respect different, i.e. the bracket base is larger than the wings. During testing in the universal testing machine, the specimen has some degree of freedom, which can result in a small angle between the bracket base and the loading direction. A small variation in loading angle may have a relatively high effect on peak stress. This was investigated with FE analysis (Figure 4). The analysis showed that variation in the loading angle and bracket base between 0 and 10 degrees resulted in a peak stress from 20.6 to 10.3 MPa, respectively. Based on the experimentally determined SBS, the angle in the experiments would have had to be approximately 7.5 degrees.

The SEM photographs and high ARI scores showed that the weakest point in the bracket–cement–enamel system was at the cement–bracket interface. The fracture patterns of the tensile test showed clear debonding between the cement and the bracket, while the shear test showed a more complex but reproducible fracture pattern. During loading, the initial stress was localized in the cement at the edge of the bracket, as shown by FE analysis. When the peak stress exceeds the bond strength between the cement and the bracket, a crack develops, which travels at this interface. At a certain point, the bracket starts to behave as a cantilever. At that moment, the loading direction changes to a combined tensile–shear force resulting in a cohesive fracture pattern. After fracture, most of the adhesive remains on the enamel interface. An explanation for this finding is the presence of more defects at the bracket side compared with the enamel side. Fractures start at locations in the bonding area where these defects are present and the stress is high (Higg *et al.*, 2001).

Conclusions

Loading a bracket at the short side resulted in significantly higher bond strength compared with loading at the long side. This could be explained by the angle of loading. The highest stress concentrations during shear loading are located at the side of loading. The obtained results were rationalized with FE analysis. The models showed a large stress non-homogeneity of the bracket–cement–enamel system during loading. The usefulness of these models was supported by the *in vitro* test results and the SEM photographs. Because of the difficulty of controlling the loading angle in most shear tests, bond strength testing for comparative reasons can be best performed in tensile rather than shear mode. Clinical improvement of bracket bond strength might be achieved by changing the bracket geometry. This should lead to a more homogeneous stress distribution within the cement layer during loading activity and therefore lower peak stresses.

References

Algera T J, Kleverlaan C J, de Gee A J, Prahl-Andersen B, Feilzer A J 2005 The influence of accelerating the setting rate by ultrasound or heat on the bond strength of glass ionomers used as orthodontic bracket cements. European Journal of Orthodontics 27: 472–476

Algera T J, Kleverlaan C J, Prahl-Andersen B, Feilzer A J 2008a The influence of different bracket base surfaces on tensile and shear bond strength. European Journal of Orthodontics 30: 490–494

Algera T J, Kleverlaan C J, Prahl-Andersen B, Feilzer A J 2008b The influence of dynamic fatigue loading on the separate components of the bracket-cement-enamel system. American Journal of Dentistry 21: 239–243

Årtun J, Bergland S 1984 Clinical trials with crystal growth conditioning as an alternative to acid-etch enamel pretreatment. American Journal of Orthodontics 85: 333–340

Geng J P, Tan K B, Liu G R 2001 Application of finite element analysis in implant dentistry: a review of the literature. Journal of Prosthetic Dentistry 85: 585–598

Haydar B, Sarikaya S, Cehreli Z C 1999 Comparison of shear bond strength of three bonding agents with metal and ceramic brackets. Angle Orthodontist 69: 457–462

Higg W A, Lucksanasombool P, Higgs R J, Swain M V 2001 Evaluating acrylic and glass-ionomer cement strength using the biaxial flexure test. Biomaterials 22: 1583–1590

Katona T R 1997 A comparison of the stresses developed in tension, shear peel, and torsion strength testing of direct bonded orthodontic brackets. American Journal of Orthodontics and Dentofacial Orthopedics 112: 244–251

Katona T R, Long R W 2006 Effect of loading mode on bond strength of orthodontic brackets bonded with 2 systems. American Journal of Orthodontics and Dentofacial Orthopedics 129: 60–64

O'Brien K D, Read M J, Sandison R J, Roberts C T 1989 A visible light-activated direct-bonding material: an *in vivo* comparative study. American Journal of Orthodontics and Dentofacial Orthopedics 95: 348–351

Walker M P, Spencer P, Eick J D 2003 Effect of simulated resin-bonded fixed partial denture clinical conditions on resin cement mechanical properties. Journal of Oral Rehabilitation 30: 837–846